Available online at www.sciencedirect.com
ScienceDirect
Applied Radiation and Isotopes 66 (2008) 1213–1217
Applied Radiation and Isotopes
www.elsevier.com/locate/apradiso

Dose–image quality study in digital chest radiography using Monte Carlo simulation

S.C.A. Correa[a], E.M. Souza[a], A.X. Silva[b,*], R.T. Lopes[a], H. Yoriyaz[c]

[a][Programa de Engenharia Nuclear]/COPPE, Universidade Federal do Rio de Janeiro, Ilha do Fundão, Caixa Postal 68509, 21945-970 Rio de Janeiro, RJ, Brazil
[b][PEN/COPPE-DNC/Poli]CT, Universidade Federal do Rio de Janeiro, Ilha do Fundão, Caixa Postal 68509, 21945-970 Rio de Janeiro, RJ, Brazil
[c]Instituto de Pesquisas Energéticas e Nucleares, CNEN, IPEN, Av. Lineu Prestes 2242, Cidade Universitária, Armando Salles Oliveira Pinheiros, Caixa Postal 11049, 05422270 São Paulo, SP, Brazil

Received 23 August 2007; received in revised form 11 January 2008; accepted 16 January 2008

Abstract

One of the main preoccupations of diagnostic radiology is to guarantee a good image-sparing dose to the patient. In the present study, Monte Carlo simulations, with MCNPX code, coupled with an adult voxel female model (FAX) were performed to investigate how image quality and dose in digital chest radiography vary with tube voltage (80–150 kV) using air-gap technique and a computed radiography system. Calculated quantities were normalized to a fixed value of entrance skin exposure (ESE) of 0.0136 R. The results of the present analysis show that the image quality for chest radiography with imaging plate is improved and the dose reduced at lower tube voltage.

Keywords: Chest radiography; Dose-image; Monte Carlo simulation

1. Introduction

Thanks to technological improvements, digital radiography is replacing conventional film-screen radiography. The operational facility such as post-processing, large dynamic range and high detective quantum efficiency makes this alternative particularly attractive.

One of the main differences of digital detectors when compared to conventional screen-film systems is their varying sensitivity to X-ray energy. Most analog systems use gadolinium-based screens with a k-edge peak sensitivity at about 50 keV, while, for instance, the BaFBr imaging plates have a k-edge peak sensitivity at approximately 37.4 keV (Rowlands, 2002). As a result, the spectral quality of the X-ray beam that will produce the best image with a digital detector is likely to be different for screen film. Since the properties of these two detector systems differ in several ways, there is obviously a need for more optimization studies including both diagnostic quality of the images and the effective dose to the patient. However, experimental optimization studies is difficult because it involves several factors such as X-ray source, scatter-rejection techniques and X-ray detector system, mainly for chest that possess structures with both high and low attenuations. Consequently, computational simulation has been considered a powerful tool to establish the correlation between the physical parameters of the imaging system and the relevant diagnostic information in the image, mainly after the creation of voxel models that are a very close representation of the human body.

The Monte Carlo code MCNP has been widely used in dosimetric studies and radiation protection for its capability to treat coupled neutron/photon/electron transport in user defined 3-dimensional geometry. With the advent of the capacity of radiographic simulation from version MCNPX (Pelowitz, 2005), the image simulation can also be obtained.

Kramer et al. (2004) has developed an adult voxel female model (FAX) phantom based on CT images of female

*Corresponding author.
E-mail address: ademir@con.ufrj.br (A.X. Silva).

0969-8043/$ - see front matter © 2008 Elsevier Ltd. All rights reserved.
doi:10.1016/j.apradiso.2008.01.009

patients, whose organ and tissue masses have been adjusted in order to correspond to the anatomical specifications defined by the ICRP Publication 89 for the Female Reference Adult (ICRP, 2003). This new phantom connected to the capacity of image simulation from Monte Carlo code MCNPX comes as a great alternative in the study of parameters that can affect the image quality in medical applications.

The purpose of this work is to use the above-mentioned Monte Carlo code MCNPX and the FAX voxel phantom, to investigate which tube potential should be used in the computed radiography (imaging plate) of the chest with an air-gap technique in order to maintain or improve image quality and still maintain patient doses at a low level.

2. Modeled system

2.1. Computer model

The calculations were made using the Monte Carlo code MCNPX version 2.5.0. The imaging system was modeled by simulating photon transport from the X-ray tube and through the phantom. The photons were transported taking into account photoelectric absorption, coherent and incoherent scattering. The number of histories simulated in all cases assures the estimated statistical error is less than 5%.

2.2. X-ray source

The initial photon energy was sampled from an X-ray spectrum pre-calculated with a program by Cranley et al. (1997), which uses the tube peak voltage, anode material, anode angle, filter material and filter thickness as input parameters. The energy distributions of X-ray used were obtained using 5.9 mm Al + 0.1 mm Cu filtration and tungsten anode material with an angle of 15°.

X-ray photons were emitted from a disk source with 3-mm diameter collimated into a cone of directions. Source biasing variance reduction technique was considered. In order to obtain a field size of $33 \times 29\,cm^2$ in the phantom skin, lead collimation of 1-cm thickness was used. The focus–detector distance used in this work was of 300 cm, moreover 30 cm air gap was added in order to reduce the scatter contribution. With this irradiation setup, chest exposures with projection geometry posterior–anterior (PA) were evaluated and images were obtained using 80–150 kV_p voltage tube range.

2.3. Voxel phantom

The voxel phantom FAX (Kramer et al., 2004) was used as a model of a patient. The FAX is 163-cm high and has a mass of 59.76 kg. It was modeled in MCNPX code utilizing the SCMS software (Yoriyaz et al., 2000), which is a computational tool for the construction of geometric or anatomic models from medical images like computerized tomography (CT), single photon emission computerized tomography (SPECT) or other similar digital images. The SCMS software interprets the images and provides an input file to be used by the Monte Carlo MCNPX code for the simulation of the radiation transport (Yoriyaz et al., 2001).

2.4. Detector

The MCNPX radiography tally is based on point detector techniques, where the radiography focal plane grid is an array of point detectors close enough to one another to generate an image based on the point detector fluxes. The resultant image is an aerial photon distribution leaving the simulated test object mapped in two dimensions, forming a virtual image or pseudo-digital image. Each detector point represents one picture element (pixel) that forms the simulate image. The gray scale of the image is produced by the number of photons passing a particular area, i.e. darker gray levels are produced when more photons are recorded.

In order to reproduce the photon absorption rate in an imaging plate system, the energy-dependent response of a BaFBr imaging plate detector was modeled and introduced in MCNPX radiography tally input. In MCNPX, this was possible using an energy-dependent multiplier to a tally (the DE and DF cards). This feature allows entering a point-wise function as a function of energy to modify the employed tally. It has been used to estimate the locally deposited energy in the BaFBr imaging plate that is the basis of the latent image formation process.

The latent image is a consequence of the energy of the X-rays absorbed. For a preliminary image quality test, independently from the characteristic of the peculiar device (that are dependent on the manufacturer), the energy trapped in the phosphor structure is the basic aspect that one should investigate. DF values for BaFBr imaging plate were obtained through a series of separate runs for a set of monoenergetic (DE) photon sources with expanded and aligned field, tallying the energy deposited in a volume of BaFBr with density of $5.1\,g\,cm^{-3}$ (Rowlands, 2002).

Fig. 1 shows the energy absorption curve obtained from BaFBr detector simulation. The energy peak absorption obtained in the simulation was 38.4 keV. The energy peak absorption from BaFBr found in the literature is between 37.4 and 40 keV (Rowlands, 2002; Tingberg and Sjöström, 2005).

2.5. Dose calculation

The absorbed dose calculation in the FAX voxel phantom was obtained using the *F8 tally and the effective dose was calculated according to the definitions given in the ICRP Publication 60 (ICRP, 1991).

For each technique were measured the air-absorbed dose in the entrance surface of the voxel phantom using a cylinder with $100\,cm^2$ surface and $180\,cm^3$ volume. The MCNPX tally used for this was the F6. Considering that there is charged particle equilibrium, the exposure and

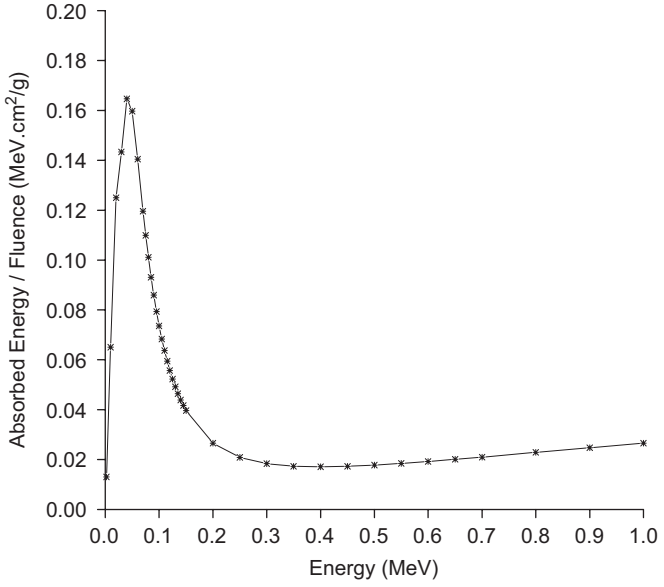

Fig. 1. Energy-absorption curve from BaFBr detector obtained in Monte Carlo simulations.

kerma were obtained through the air-absorbed dose (Attix, 1986).

2.6. Image quality

The signal-difference-to-noise ratio (SdNR) for the single-exposure method (Samei et al., 2005) was used as the measure of physical image quality. This quantity is defined as

$$\mathrm{SdNR} = \frac{|I_B - I_L|}{\sigma_B}, \quad (1)$$

where I_L and I_B refer to the intensities of the detector signal corresponding to a lesion and its background surrounding, respectively, and σ_B is the standard deviation of quantum noise in the background area. I_B and I_L are defined as

$$I_B = \langle B(m,n)\rangle \qquad I_L = \langle L(i,j)\rangle, \quad (2)$$

where $L(i,j)$ and $B(m,n)$ refer to small regions (ROI) defined within the areas of the simulated detail and the background, respectively, and i, j, m and n are coordinates of the pixels in the images defining the ROIs. The nomenclature $\langle x \rangle$ refers to the mean value of the quantity x inside the bracket averaged over the ROI. Quantum noise within the background region is defined as

$$\sigma_B = \left(\frac{1}{(MxN) - 1} \sum_{m,n} (B(m,n) - \langle B(m,n)\rangle)^2 \right)^{0.5}, \quad (3)$$

where M and N are the matrix dimensions of the background ROI, $B(m,n)$. The figure of merit (FOM) is then calculated as the square of Eq. (1) divided by the effective dose, E,

$$\mathrm{FOM} = \frac{\mathrm{SdNR}^2}{E}. \quad (4)$$

Image quality was computed for a set of cylindrical details with 10-mm diameter included in the voxel phantom at a specified location according to Fig. 2. Table 1 gives the detail thickness and composition used in the calculations.

3. Results

Results showed that the SdNR in different parts of the images varied considerably with tube voltage. Fig. 3 illustrates this for images recorded with the 300-cm FDD (focus–detector distance) and air-gap technique. The greatest change in SdNR occurred in the pleural margin region where there was 31% difference between the 80 and 150 kV_p images. The smallest change occurred in the visualization of the blood in the lung region (7% difference).

A similar trend of decrease of SdNR with the increase of the voltage was seen for most of the details, except for bone behind the heart and blood in the retrocardiac regions, which presented better results for 100–120 and 100–140 kV_p ranges, respectively.

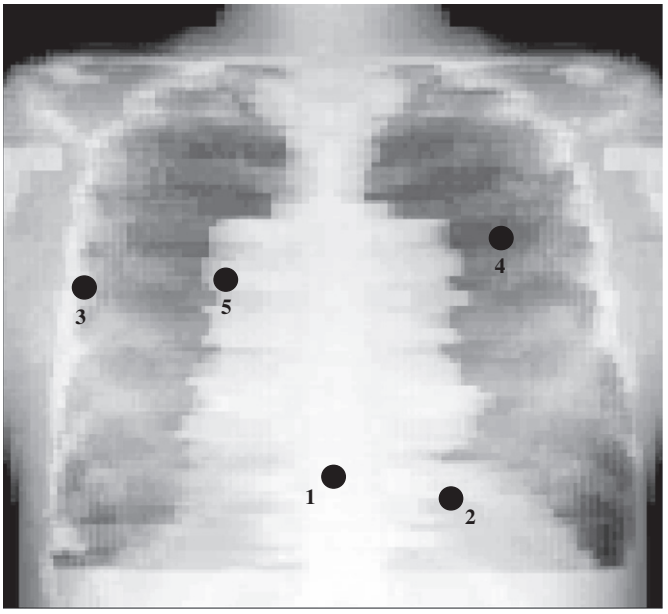

Fig. 2. The locations of the details (indicated by black solid circles) included in the voxel phantom which were used in the simulations.

Table 1
Structures used in the model calculations

Detail	Thickness (mm)	Composition	Region
1	1	Bone	Lower mediastinal (behind heart)
2	2	Blood	Retrocardial
3	1	Soft tissue	Pleural margin
4	2	Blood	Lung
5	2	Blood	Hilar

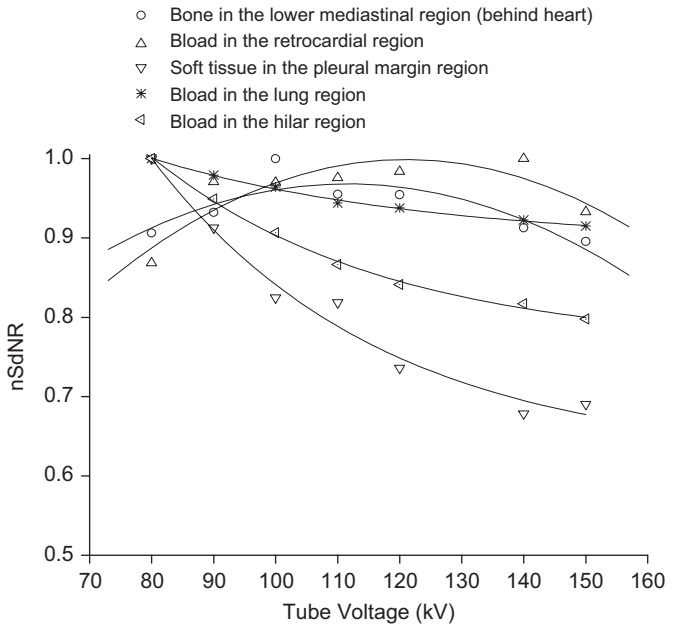

Fig. 3. Variation in SdNR for different details of images of the chest phantom with tube voltage, for the 300-cm FDD air-gap technique. *n*SdNR corresponds to the SdNR value divided for the largest value of SdNR found for each detail.

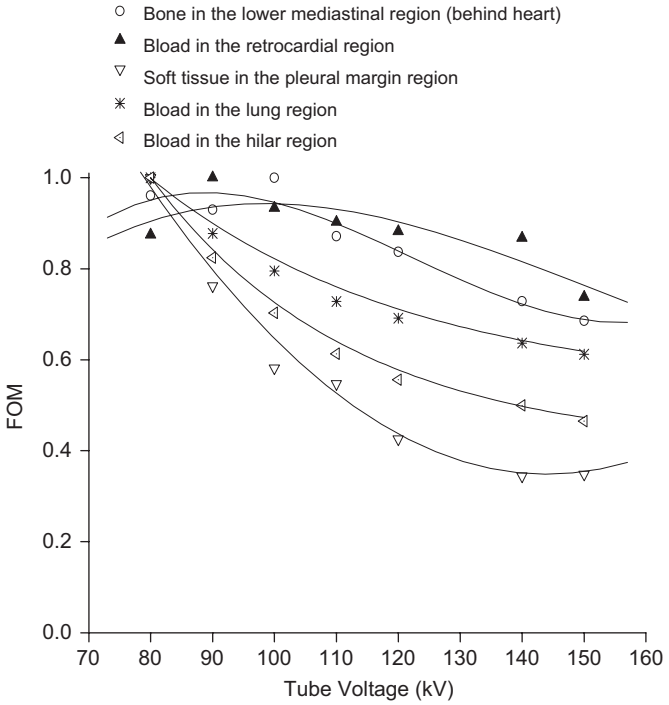

Fig. 4. FOM ($SdNR^2$ per effective dose) as a function of kVp. *n*FOM corresponds with the FOM value divided for the largest FOM value found for each detail.

A figure of merit was used to assist in evaluating which tube voltage achieved the optimum balance between the diagnostic image and the dose to patient with the chest phantom image. Fig. 4 shows the variation in the FOM with tube voltage for the evaluated details.

The results show that the clinical image quality is increased when the tube voltage is reduced for most of the details. The bone behind the heart and blood in the retrocardiac region presents an increase in visualization with the decrease of the tube voltage for voltages smaller than 120 kV. At 80 kV tube voltage, there is a decline in the image quality. Similar behavior was observed by Doyle et al. (2005) for digital chest radiography with air gap and 60–133 kV voltage tube range. In this work, the visibility of details within the lung is best at lower voltages, but for details within the heart region, intermediate voltages give better results.

In the present work, the effective dose is smaller for low tube voltages (as displayed in Fig. 5), while the air kerma in the entrance surface of the voxel phantom generally decreases with the increase of the voltage (Fig. 6).

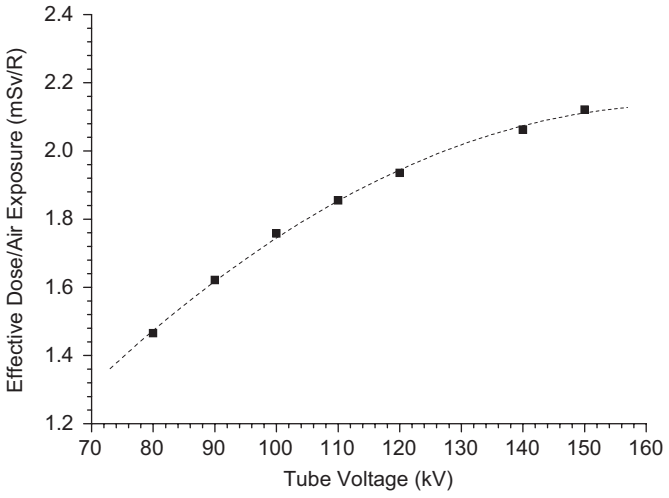

Fig. 5. Variation in effective dose with tube voltage.

4. Discussion

The current study for the chest, indicates that the clinical image quality is improved and the effective dose reduced when decreasing the kV_p for digital systems using image plates. These results are completely different from the one found in screen-film radiography (Säbel and Aichinger, 1996) where the quality of the chest image increases with tube voltages and the dose in the patient is reduced. However, for image plates the situation is reversed; the efficiency of the image plate is higher for lower photon energies. A reduction in tube voltage results in more photons being detected. The k-edge of the image plate (BaF) is at lower photon energy than it is for rare earth screens (Gd_2O_2S) (Yaffe and Rowlands, 1997) and in rare-earth screens, the dose needed to reach an optical density of 1.0 is lower at higher tube voltages (Säbel and Aichinger, 1996). These facts imply that it would be possible to improve the image quality by reducing the tube voltage for computerized radiography.

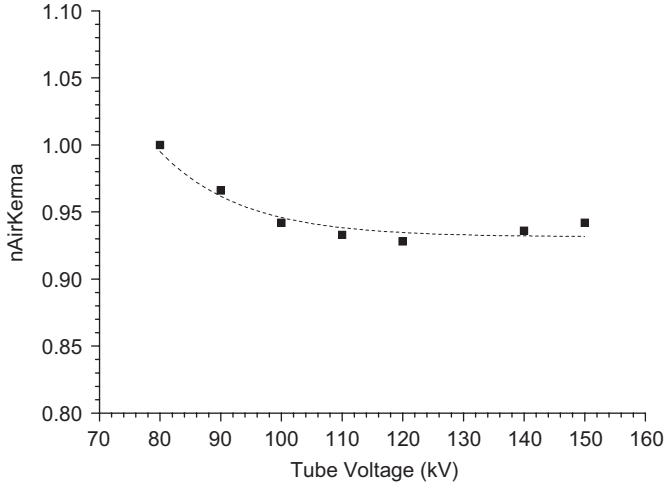

Fig. 6. Air kerma behavior at the entrance surface of the voxel phantom. *n*AirKerma corresponds to the air kerma value divided for the largest value of air kerma found.

At a low tube voltage, there will be a stronger dose gradient from the entrance surface to the exit surface compared with the situation at a higher tube voltage. At a higher tube voltage, the dose distribution will be more uniform. For a lower tube voltage, the dose at the entrance surface of the voxel phantom will be higher than that of the higher tube voltage, but it will be somewhat made up for by the fact that the dose at the exit side will be lower. In Fig. 5, the air kerma at the entrance surface of the voxel phantom is calculated for the exposure situations presented in this paper. The values obtained show that the air kerma at the entrance surface of the phantom increases when the tube voltage is decreased as expected. Since the dose at the entrance surface of the phantom is lower at higher tube voltages, it is a common misunderstanding that the effective dose is automatically reduced with a higher KV setting. In image plate radiography, a reduced dose at the entrance surface of the phantom can thus result in a higher effective dose to the patient.

Previous studies support the results of the current study. Launders et al. (2001) showed that the image quality per effective dose unit in chest radiography was improved with decreased tube voltage for a digital system based on amorphous selenium detectors. Launders et al. (2001) also point out that since the entrance surface dose decreases with increasing kVp, this argument is often used to persuade radiology departments to use high-kV settings.

Tingberg and Sjöström (2005) found that, based on a visual grading analysis (VGA) study of chest images at equal effective dose for a digital system based on image plate detector, the average VGA-score made by a group of radiologists increased with decreasing tube voltage, and Lee et al. (2005) using the MCNP Monte Carlo code and an adult hermaphrodite mathematical phantom found that the effective dose increases for higher tube voltages in chest and abdomen X-ray exams.

5. Conclusion

The present analysis showed that for low tube voltage, the image quality for chest in imaging plates is improved and the dose reduced. Those results confirm that the MCNPX radiography tally coupled to FAX voxel phantom are useful in the study of parameters that can affect the image quality and dose to the patient.

Acknowledgments

The authors wish to thank the financial support of the Conselho Nacional de Desenvolvimento Científico e Tecnológico (CNPq) and Fundação Carlos Chagas Filho de Amparo à Pesquisa do Estado do Rio de Janeiro (FAPERJ), Brazil.

References

Attix, F.H., 1986. Introduction to Radiological Physics and Radiation Dosimetry. New York, Wiley.

Cranley, K., Gilmore, B.J., Fogarty, G.W.A., Desponds, L., 1997. Catalogue of diagnostic X-ray spectra and other data. Report 78, The Institute of Physics and Engineering in Medicine.

Doyle, P., Martin, C.J., Gentle, D., 2005. Dose–image quality optimisation in digital chest radiography. Radiat. Prot. Dosimetry 114, 269–272.

International Commission on Radiological Protection, 1991. Recommendations of the International Commission on radiological protection. ICRP Publication 60, Pergamon Press, Oxford.

International Commission on Radiological Protection, 2003. Basic anatomical and physiological data for use in radiological protection: reference values. ICRP Publication 89, Pergamon Press, Oxford.

Kramer, R., Khoury, H.J., Vieira, J.W., Loureiro, E.C.M., Lima, V.J.M., Lima, F.R.A., Hoff, G., 2004. All about FAX: a female adult voxel phantom for Monte Carlo calculation in radiation protection dosimetry. Phys. Med. Biol. 49, 5203–5216.

Launders, J.H., Cowen, A.R., Bury, R.F., Hawkridge, P., 2001. Towards image quality, beam energy and effective dose optimisation in digital thoracic radiography. Eur. Radiol. 11, 870–875.

Lee, S.C., Wang, J.N., Liu, S.C., Jiang, S.H., 2005. Effective dose evaluation for chest and abdomen X-ray tests. Radiat. Prot. Dosimetry 116, 613–619.

Pelowitz, D.B., 2005. MCNPX^{TM} User's Manual, Version 2.5.0. LA-CP-05-0369, Los Alamos National Laboratory.

Rowlands, J.A., 2002. The physics of computed radiography. Phys. Med. Biol. 47, 123–166.

Säbel, M., Aichinger, H., 1996. Automatic exposure control. In: Gfirtner, H., Moores, B.M., Schmidt, T., Schibilla, H. (Eds.), Quality Assurance and Patient Radiation Protection in Diagnostic Radiology. H. Hoffmann GMBH Verlag, Berlin.

Samei, E., Dobbins III, J.T., Lo, J.Y., Tomai, M.P., 2005. A framework for optimising the radiographic technique in digital X-ray imaging. Radiat. Prot. Dosimetry 114, 220–229.

Tingberg, A., Sjöström, D., 2005. Optimization of image plate radiography with respect to tube voltage. Radiat. Prot. Dosimetry 114, 286–293.

Yaffe, M.J., Rowlands, J.A., 1997. X-ray detectors for digital radiography. Phys. Med. Biol. 42, 1–39.

Yoriyaz, H., Santos, A., Stabin, M., 2000. Absorbed fractions in a voxel-based phantom calculated with the MCNP-4B code. Med. Phys. 27, 1555–1562.

Yoriyaz, H., Stabin, M., dos Santos, A., 2001. A Monte Carlo MCNP-4B based absorbed dose distribution estimates for patient-specific dosimetry. J. Nucl. Med. 42, 662–669.